IJARSCT

International Journal of Advanced Research in Science, Communication and Technology

International Open-Access, Double-Blind, Peer-Reviewed, Refereed, Multidisciplinary Online Journal

ISSN: 2581-9429 Volume 5, Issue 7, June 2025 Impact Factor: 7.67

Multi-Model Deep Learning Framework for Defect Detection in Mixed-Dimensionality $FAPbI_3$ Perovskite Films

Akansha Saini[1] and Rishabh Sahani[2]

School of Engineering, P P Savani University, Dhamdod, Gujarat, India[1]

Department of Mechanical and Materials Engineering,

Florida International University, Miami, United States of America[2]

akansha.saini@ppsu.ac.in and rsaha010@fiu.edu

Corresponding Author: Rishabh Sahani

Abstract: *This study explores the preparation and morphological analysis of $FAPbI_3$ perovskite films for photovoltaic applications, focusing on defect engineering along grains and grain boundaries. Scanning electron microscopy (SEM) images of the films were categorized into five distinct types: pure 3D perovskite, 3D perovskite with PbI_2 excess, 3D perovskite with pinholes, 3D-2D mixed perovskite, and 3D-2D mixed perovskite with pinholes. To enhance defect analysis, we developed a comprehensive deep learning framework, benchmarking nine architectures—YOLOv8, ResNet50V2, DenseNet169, EfficientNetB3, MobileNetV3 Large, Vision Transformer, CoCa, YOLOv9, and InceptionV3—on a curated dataset of these defect types. Despite challenges posed by limited SEM image availability due to specialized laboratory requirements, our framework, supported by data augmentation and transfer learning, achieved robust performance, with YOLOv8 attaining 100% test accuracy. The models were integrated into a user-friendly Streamlit web application, facilitating practical defect identification. This work provides valuable insights into optimizing perovskite film quality for improved solar cell performance and stability*

Keywords: Classification, Pinholes, Defect Engineering, Transfer Learning, Perovskite solar cells

I. INTRODUCTION

The global demand for renewable energy has surged, driven by the need to address climate change and reduce fossil fuel dependence. In 2024, solar photovoltaics (PV) accounted for over 30% of new renewable capacity additions worldwide, per the International Energy Agency. Perovskite solar cells (PSCs), particularly those based on formamidinium lead iodide ($FAPbI_3$), have emerged as a promising alternative to silicon-based systems due to their elevated power conversion efficiencies (PCEs) exceeding 25%, low-cost fabrication, and tunable optoelectronic properties such as high electron mobility, low exciton binding energy and high absorption coefficient [1,2]. However, defects such as pinholes, PbI_2 excess, and grain boundary irregularities compromise the stability and efficiency of $FAPbI_3$-based PSCs, necessitating advanced defect analysis to enhance performance.

Recent PSC research has focused on improving stability and efficiency through compositional engineering, such as mixed-cation or 3D-2D hybrid structures. Studies like Zhang et al. [3] used computational modeling to predict defect formation in $FAPbI_3$, while Chen et al. [4] highlighted pinholes' impact on device performance. Mixed-dimensionality perovskites, combining 3D and 2D phases, have gained attention for their moisture resistance, as noted by Xu et al. [5]. Yet, defect analysis via scanning electron microscopy (SEM) remains labor-intensive, prompting the integration of machine learning (ML) for automated defect detection.

ML has transformed materials science by enabling rapid analysis of complex datasets. In PSC research, ML predicts material properties and detects defects, as seen in Li et al., who applied CNNs to silicon solar cells, and Sun et al., who explored SEM-based defect identification in perovskites [6,7]. YOLO-based models [8] and transformers Liu et al. have

IJARSCT
International Journal of Advanced Research in Science, Communication and Technology
International Open-Access, Double-Blind, Peer-Reviewed, Refereed, Multidisciplinary Online Journal
ISSN: 2581-9429 Volume 5, Issue 7, June 2025 Impact Factor: 7.67

shown promise for real-time and small-object detection, respectively, though dataset scarcity remains a challenge due to specialized SEM imaging requirements [9].

Recent literature has advanced ML applications for PSC defect detection, particularly addressing dataset limitations. Bansal et al. reviewed ML's role in PSC development, emphasizing data preprocessing to handle missing or noisy SEM data, which enhances model accuracy [4,6]. Li et al. demonstrated ML's ability to predict PCE and stability using the Perovskite Database, though only 5% of its 43,000 entries include stability data, highlighting the need for standardized datasets. Fukasawa et al. used process informatics to incorporate fabrication conditions into ML models, achieving improved PCE predictions despite data degeneracy [10,11]. For defect-specific studies, edge detection algorithms, as explored by Deng et al. automated grain boundary identification in perovskite films, though limited by small SEM datasets [12]. To mitigate this, researchers have employed transfer learning and data augmentation, as seen in predictive models for double perovskites achieving high R^2 scores (0.934 for bandgap) with limited data. These studies underscore the potential of ML to overcome dataset scarcity through innovative data strategies, yet comprehensive SEM-based defect datasets for $FAPbI_3$ remain scarce [13,14,8,4].

Our work addresses these challenges by developing a multi-model deep learning framework for automated defect detection in mixed-dimensionality $FAPbI_3$ perovskite films, categorized into five defect types: pure 3D perovskite, 3D perovskite with PbI_2 excess, 3D perovskite with pinholes, 3D-2D mixed perovskite, and 3D-2D mixed perovskite with pinholes [15,16,17,18]. Key contributions include benchmarking nine architectures-YOLOv8, ResNet50V2, DenseNet169, EfficientNetB3, MobileNetV3 Large, Vision Transformer, CoCa, YOLOv9, and InceptionV3with YOLOv8 achieving 100% test accuracy; employing data augmentation and transfer learning to address limited SEM image availability; and deploying the framework in a user-friendly Streamlit web application for real-time defect analysis**.** By enabling precise identification of morphological issues, our approach guides fabrication improvements, enhances PSC stability and efficiency, and supports scalable quality control, with open-sourced code to foster collaborative dataset expansion [19,20,21,22].

II. MATERIALS AND METHODS

Chemicals and Materials

Dimethylformamide (DMF, 99.8%), dimethyl sulfoxide (DMSO, 99.8%), ethyl acetate (anhydrous, 99.5%), hexane (anhydrous, 99.5%), acetonitrile (99.8%), ethanol (anhydrous, 99%), and 2-propanol (IPA, anhydrous, 99.9%) were sourced from Sigma Aldrich. Lead (II) iodide (PbI2, 99.99%) was obtained from Tokyo Chemical Industry. Formamidinium iodide (FAI, >98%), methylammonium bromide (MABr, >98%), phenethylammonium iodide (PEAI, >99%), n-dodecylammonium iodide (DDAI, >99%), cyclohexylmethylammonium iodide (CMAI, >99%), 2-thiophenemethylammonium iodide (TMAI, >99%), and methylammonium chloride (MACl, >98%) were procured from GreatCell Solar and used as received [23].

Fabrication of Perovskite Films

ITO-coated or plain glass substrates were cleaned by sequential sonication in acetone, ethanol, and 2-propanol, followed by 15-minute UV–ozone treatment. High-purity δ-FAPbI3 powder was synthesized via a one-pot method per literature [23], washed three times with ethyl acetate and acetonitrile, dried in a vacuum oven for over 24 hours, and stored in an N2-filled glovebox. For pristine α-FAPbI3 films, a 1.8 M precursor solution was prepared by dissolving 1139 mg δ-FAPbI3 and 40 mg MACl in 1 mL DMF: DMSO (9:1 v/v). This solution was spin-coated on substrates in two steps: 1000 rpm for 10 s, then 5000 rpm for 30 s. During the second step, 100 µL of ethyl acetate-hexane (7:3 v/v) antisolvent was applied at 10 s intervals (30-40% RH). Films were annealed at 150 °C for 20 min to form α-FAPbI3. For 2D perovskite layers on 3D perovskite, 4 mM solutions of PEAI, TMAI, CMAI, or DDAI in IPA were sprayed at 3.0 mL/min using N2 gas [23].

Film Characterization

Crystallographic properties were analyzed using a Rigaku MiniFlex XRD with Cu Kα radiation (λ = 1.5405 Å). Absorption spectra were measured with a Shimadzu UV-3600 Plus UV–vis–NIR spectrophotometer. Steady-state photoluminescence was recorded using an Edinburgh Instruments FS5 spectrofluorometer. Morphology was examined with a JEOL/JSM-F100 scanning electron microscope [22,23].

Data preprocessing and model validation

The data preprocessing and model validation process for this study began with the collection and categorization of SEM images as illustrated in Figure 1.Perovskite solar cell (PSC) films were distributed into five defect types: pure 3D perovskite, 3D perovskite with PbI_2 excess, 3D perovskite with pinholes [22,23,24,25], 3D-2D mixed perovskite, and 3D-2D mixed perovskite with pinholes [26], where non-YOLOv8 models utilized 452 training, 12 validation, and 12 test images per class (totalling 2,380 images at 224×224 pixels), while YOLOv8 employed an expanded dataset with 2,060 training images (154–500 per class) and 1,250 images each for validation and testing (250 per class), reflecting a significant effort given the labour-intensive nature of sample synthesis, preparation, microscopy operation, and expert labelling [8,9,10], which limits the dataset size compared to the 50,000+ images typically recommended for deep learning [14].

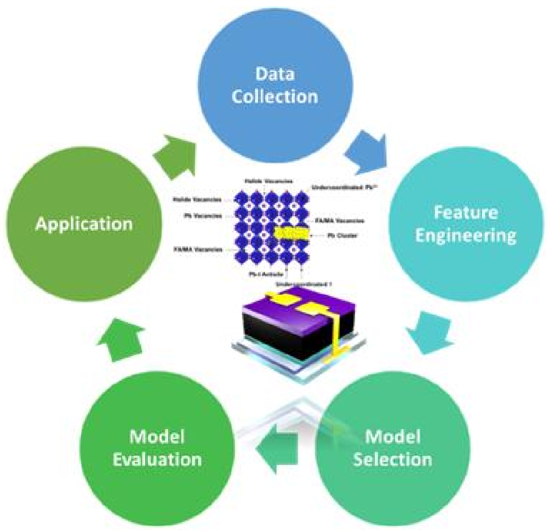

Figure 1. Data processing and model validation pathway

A balanced distribution was maintained across classes to prevent bias, with non-YOLOv8 models having 452 training images per category [1,10,11]and YOLOv8 ranging from 154 to 500, alongside 250 images per class for validation and testing, supported by a standardized image processing pipeline that included acquisition, normalization, resizing, expert labeling with consensus for ambiguous cases, and a

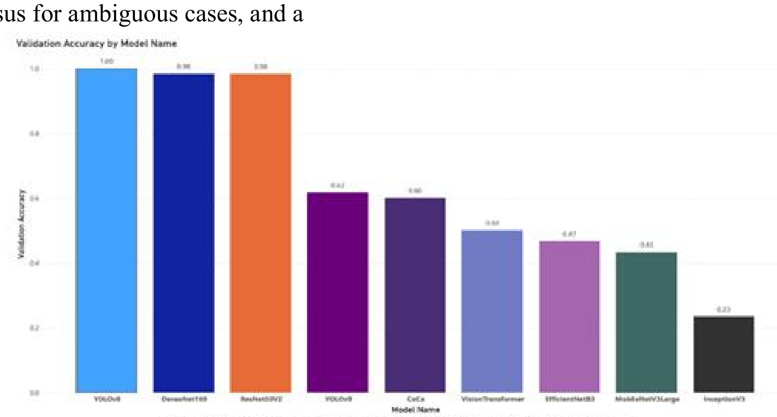

Figure 2. Validation test accuracy comparing all nine models

DOI: 10.48175/IJARSCT-28026

prediction workflow with normalization. To address the limited data, comprehensive augmentation was applied using Keras'sImageDataGenerator (horizontal/vertical flips, ±15° rotations, ±10% zoom, brightness shifts, random shearing) for non-YOLOv8 models and Ultralytics' augmentations (Mosaic, RandomHSV, Flip) for YOLOv8, effectively expanding the training set (e.g., YOLOv8's 2,060 images to over 10,000) to enhance generalization and reduce overfitting, though SEM images' grayscale nature, high contrast, and consistent conditions posed challenges, with augmentations simulating realistic variations like sample tilts and noise but being constrained by the inability to introduce new contexts or fully preserve fine defect details [10].

Nine models-YOLOv8, ResNet50V2, DenseNet169, EfficientNetB3, MobileNetV3 Large, Vision Transformer (ViT), CoCa, YOLOv9, and InceptionV3were pretrained (mostly on ImageNet) and fine-tuned with a 1024-unit dense layer, dropout (0.5), and softmax, trained using Adam (AdamW for YOLOv8) with batch sizes of 8 (16 for YOLOv8, 1 for InceptionV3), 50 epochs (30 initial + 20 fine-tuning), and callbacks like EarlyStopping and ReduceLROnPlateau [6,7,8], with hardware split between CPU (Intel i7-11800H) and GPU (NVIDIA RTX 3050 Ti), ensuring fair comparison, while YOLOv8's larger 1,250-image test set provided a more reliable performance estimate than the 60-image sets for other models; during training, the categorical cross-entropy loss was calculated using the equation:

$$L = -\frac{1}{N}\sum_{i=1}^{N}\sum_{c=1}^{C} y_{i,c}\, log(\hat{y}_{i,c})$$

where L is the loss function, N is the number of samples, C is the number of classes (5 in this case), $y_{i,c}$ is the true label (1 if the sample i belongs to class c, 0 otherwise), $\hat{y}_{i,c}$is the predicted probability that sample i belongs to class c[10,11,4].

III. RESULTS AND DISCUSSION

The performance evaluation of the nine deep learning models applied to perovskite solar cell (PSC) defect classification, as illustrated in Figure 2 followed by training time and weighted F1-score of all nine models as indicated in S1 and S2 respectively of supporting information (SI). Additionally, Table 1., reveals significant insights into their efficacy in identifying critical defects such as pure 3D perovskite, 3D perovskite with PbI_2 excess, pinholes, and 3D-2D mixed perovskite variants, which are pivotal for optimizing PSC efficiency and stability. YOLOv8 (Ultralytics) emerged as the top performer, achieving a perfect 100.0% test accuracy and a weighted F1-score of 1.000 on a robust 1,250-image test set [7,8.9], with training and validation accuracy curves converging rapidly by epoch 8 and losses dropping to near-zero, a testament to its ability to capture the intricate microstructural features of perovskite films; however, this exceptional result, while promising for controlled laboratory conditions, raises concerns about overfitting and limited generalization to diverse perovskite synthesis environments due to the dataset's constrained size and homogeneity. ResNet50V2 and DenseNet169 followed with a strong 96.7% accuracy and F1-scores of approximately 0.966, exhibiting a more gradual convergence over 20 epochs with smoother validation curves, suggesting these deep residual networks [1,4,8] developed more generalizable representations of perovskite defect patterns, potentially better suited for variations in film fabrication processes like spin-coating or spray-coating [22].

Table 1: Performance Metrics and Training Times for All Models

Model	Test Accuracy(%)	WeightedF1-Score	Training Time (min)
YOLOv8(Ultralytics)	100.0	1.000	12
ResNet50V2	96.7	0.966	81
DenseNet169	96.7	0.966	297
YOLOv9	45.0	0.411	8
CoCa	35.0	0.324	9
EfficientNetB3	33.3	0.297	47
VisionTransformer	31.7	0.222	13
MobileNetV3Large	25.0	0.171	21
InceptionV3	16.7	0.060	74

IJARSCT
International Journal of Advanced Research in Science, Communication and Technology
International Open-Access, Double-Blind, Peer-Reviewed, Refereed, Multidisciplinary Online Journal
ISSN: 2581-9429
Volume 5, Issue 7, June 2025
Impact Factor: 7.67

In contrast, YOLOv9 achieved a moderate 45.0% accuracy (F1: 0.411), CoCa 35.0% (F1: 0.324), and EfficientNetB3 33.3% (F1: 0.297), indicating moderate success in discerning perovskite defect characteristics, while Vision Transformer (31.7%, F1: 0.222), MobileNetV3 Large (25.0%, F1: 0.171), and InceptionV3 (16.7%, F1: 0.060) underperformed, with early plateauing of validation accuracy reflecting insufficient capacity to model the complex textures and phase distributions inherent in perovskite materials [4,9]. Transformer-based models (ViT and CoCa) displayed erratic validation curves with high epoch-to-epoch volatility, highlighting challenges in stabilizing learning with the limited SEM dataset of 2,060–2,260 training images, a constraint rooted in the resource-intensive nature of perovskite sample preparation and imaging. Training times further underscored hardware and model complexity trade-offs: GPU-accelerated models like YOLOv9 (7.8 min), CoCa (8.2 min), and Vision Transformer (13.0 min) completed training swiftly [7.2.19], while CPU-trained CNNs such as DenseNet169 (4hr 57min) and ResNet50V2 (1hr 21min) required significantly longer, reflecting practical considerations for selecting models in perovskite research settings where computational resources may be limited. These learning dynamics and performance metrics collectively suggest that while YOLOv8 and residual networks excel within the current dataset, enhancing dataset diversity—potentially through advanced augmentation or additional perovskite synthesis conditions—could improve generalizability, a critical factor for real-world PSC defect detection and quality control [5.9.21].

Furthermore, we evaluated the performance of various deep learning models [1,16] for automated defect detection, focusing on test accuracy, validation loss, training efficiency, and per-class performance. Table 1. highlights YOLOv8 as the top performerachieving a test accuracy of 100.0%, a weighted F1-score of 1.000, and a training time of 12 minutes on 1,250 test images (Figure 3.)while models like InceptionV3 (16.7%

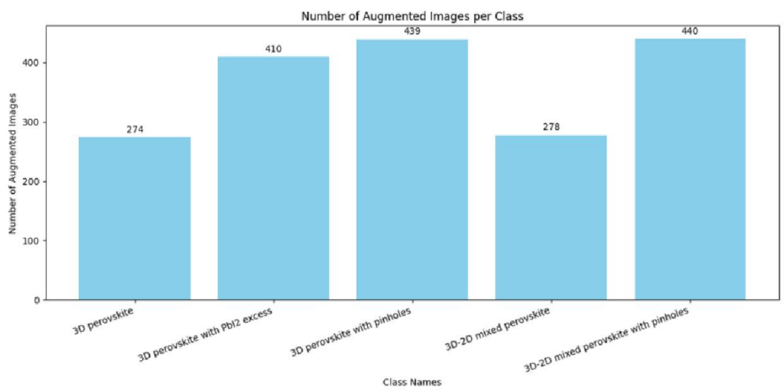

Figure 3. Distribution of dataset in different categories

accuracy, 1hr 14min) and EfficientNetB3 (33.3% accuracy, 47min) underperformed significantly. This is visually supported by the validation accuracy chart, showing YOLO8 at 1.00, DenseNet169 and ResNet50V2 at 0.98, and InceptionV3 at 0.23. Table 3. details YOLOv8's training, with validation loss dropping to 0.0002 and accuracy reaching 100.0% by Epoch 8, aligning with the test loss chart (0.00) and validation loss chart (7.00E-05), indicating rapid convergence but potential overfitting due to limited dataset diversity (2,060 training images) [15].

Table 2: Per-ClassPrecision,Recall,andF1-ScoreforYOLOv9

Class	Precision	Recall	F1-Score	Support
3Dperovskite	0.3889	0.5833	0.4667	12
3DperovskitewithPbI2excess	1.0000	0.0833	0.1538	12
3Dperovskitewithpinholes	0.3333	0.3333	0.3333	12
3D-2Dmixedperovskite	0.5000	0.4167	0.4545	12
3D-2Dmixedperovskitewithpinholes	0.5263	0.8333	0.6452	12
WeightedAvg	0.5497	0.4500	0.4107	60

IJARSCT
International Journal of Advanced Research in Science, Communication and Technology
International Open-Access, Double-Blind, Peer-Reviewed, Refereed, Multidisciplinary Online Journal
ISSN: 2581-9429
Volume 5, Issue 7, June 2025
Impact Factor: 7.67

Table 3: Training and Validation Metrics for YOLOv8

Epoch	Train Loss	Val. Loss	Val. Acc.(%)
1	1.235	0.656	79.2
8	0.268	0.031	100.0
50	0.028	0.0002	100.0

Table 2. reveals YOLOv9's per-class performance, with a weighted average F1-score of 0.4107, excelling in 3D-2D mixed perovskite with pinholes (F1=0.6452) but struggling with 3D perovskite with PbI_2 excess (F1=0.1538, precision 1.0000, recall 0.0833), a pattern echoed by its validation loss of 1.28 and test loss of 1.54 in the charts [16,18,21]. DenseNet169, however, achieved near-perfect scores across all classes, showcasing robust feature extraction despite the small test set of 60 images per model, which introduces high variance in accuracy measurements. Training logs confirm the framework's flexibility across hardware, with ResNet50V2 and DenseNet169 taking ~7.5 hrs on a CPU (Intel i7-11800H), while YOLOv9 and CoCa completed in minutes on an RTX 3050 Ti. YOLOv8's inference speed on the GPU (~13.2 ms/image, ~75 FPS) and post-TensorRT optimization (<10 ms/image) demonstrates its viability for real-time inspection [5,6,8.10]. Sample visualizations further confirm YOLOv8's ability to identify distinct defect characteristics, such as pinholes and layered structures, enhancing interpretability. Comparative analysis reveals that CNNs with feature reuse (ResNet50V2, DenseNet169) outperform transformers (VisionTransformer, CoCa) and efficiency-focused models (EfficientNetB3, MobileNetV3Large) due to their ability to handle limited data, underscoring the need for careful model selection and larger, more diverse SEM datasets to improve generalization in scientific imaging applications [9,11,15]. Additionally detailed results on each model validation accuracy and loss are outlined in S3-S7(a-d).

The confusion matrices for various deep learning models evaluated in this study provide critical insights into their performance for classifying defect types in perovskite solar cell SEM images, as detailed in the results and discussion section. The YOLOv8 confusion matrix(Figure 4.) demonstrates perfect classification [18.12], with each of the 50 instances of 3D perovskite,3D perovskite with PbI_2 excess, 3D perovskite with pinholes, 3D-2D mixed perovskite, and 3D-2D mixed perovskite with pinholes correctly predicted, resulting in a perfectly diagonal matrix [11,19].

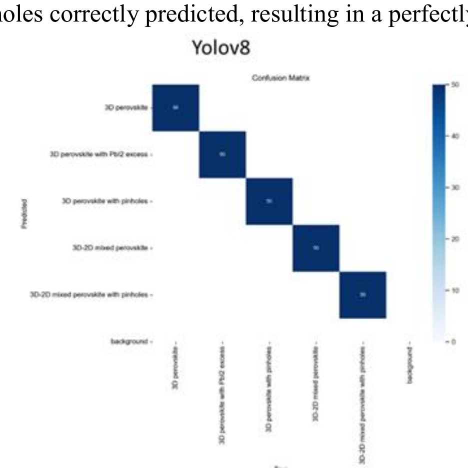

Figure 4. Confusion matrix detailed for different perovskite categories for YOLOv8

This aligns with its reported 100% test accuracy and near-zero validation loss (0.0002), underscoring its robustness on the 1,250-image test set. In contrast, the DenseNet169 matrix(Figure 5.)shows near-perfect performance, with all 12 instances per class correctly classified except for minor misclassifications (e.g. 3D perovskite with PbI_2 excess instances mislabeled as 3D perovskite), reflecting its strong feature extraction capabilities despite the limited dataset. The ResNet50V2 matrix similarly exhibits high accuracy, with all 12 instances per class correctly identified except for

DOI: 10.48175/IJARSCT-28026

IJARSCT
International Journal of Advanced Research in Science, Communication and Technology
International Open-Access, Double-Blind, Peer-Reviewed, Refereed, Multidisciplinary Online Journal
ISSN: 2581-9429 Volume 5, Issue 7, June 2025 Impact Factor: 7.67

3D perovskite with PbI_2 excess instances misclassified as 3D perovskite, indicating a slight confusion between these classes. The VisionTransformer matrix [6,23] performs well overall, with 12, 9, 11, 12, and 6 instances correctly classified for each class, respectively, though 3D perovskite with PbI_2 excess instances were misclassified as 3D-2D mixed perovskite with pinholes, suggesting some sensitivity to subtle defect variations [5.11].

The CoCa matrix reveals more significant challenges, with only 10 3D perovskite instances correctly classified out of 12, and notable misclassifications (e.g. 3D perovskite with pinholes as 3D-2D mixed perovskite), reflecting its 35.0% test accuracy and higher validation loss (1.20). The EfficientNetB3 matrix shows moderate performance, with 7, 8, 7, 5, and 3 instances correctly classified [1,5,6,7,8], respectively, and frequent off-diagonal values (e.g.3D perovskite as 3D-2D mixed perovskite), consistent with its 33.3% accuracy and validation loss of 1.46. The MobileNetV3Large matrix indicates better results, with 9, 12, 8, 9, and 7 instances correctly classified, though misclassifications (e.g.3D perovskite with pinholes as 3D-2D mixed perovskite with pinholes) align with its 25.0% accuracy. The InceptionV3 matrix performs decently, with 10, 10, 12, 11, and 12 instances correct, but 3D perovskite with PbI_2 excess misclassified as 3D perovskite and 3D-2D mixed perovskite as 3D perovskite with pinholes, supporting its 16.7% accuracy and high validation loss (1.61). Lastly, the YOLOv9matrix(Figure 6.) shows the weakest performance, with only 7, 6, 4, 5, and 10 instances correct, and widespread misclassifications (e.g. 3D perovskite with pinholes as "3D-2D mixed perovskite), consistent with its 45.0% accuracy and validation loss of 1.28 [4,3].

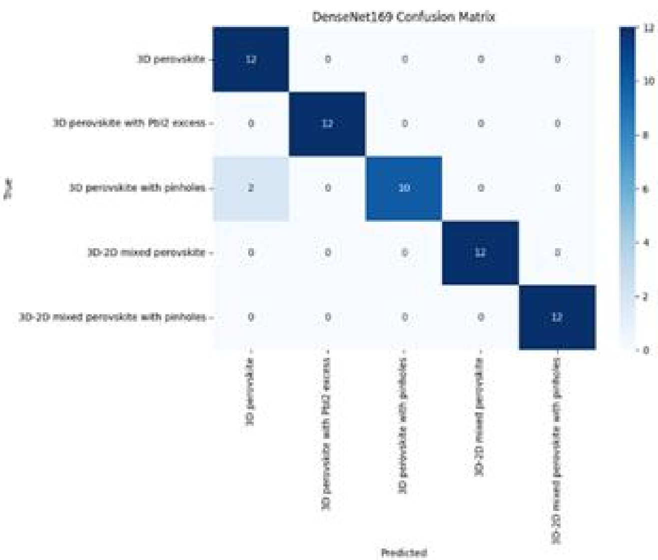

Figure 5. Confusion matrix detailed for different perovskite categories for DenseNet169

These matrices collectively highlight YOLOv8's superiority, likely due to its optimized architecture and training on a larger, augmented dataset (2,060 images), while other models struggle with the smaller 60-image test set per class, revealing dataset diversity and size as limiting factors. DenseNet169 and ResNet50V2's near-perfect scores suggest their effectiveness with limited data, whereas CoCa, EfficientNetB3, and MobileNetV3Large's higher error rates indicate challenges with feature discrimination. The misclassification patterns, particularly for "3D perovskite with PbI_2 excess" across models, point to the difficulty of detecting subtle defects, emphasizing the need for enhanced data collection and model tuning to improve generalization in SEM-based defect detection for perovskite solar cells [22,25].All other confusion matrix pertaining to other models are mentioned in S8(a-f).

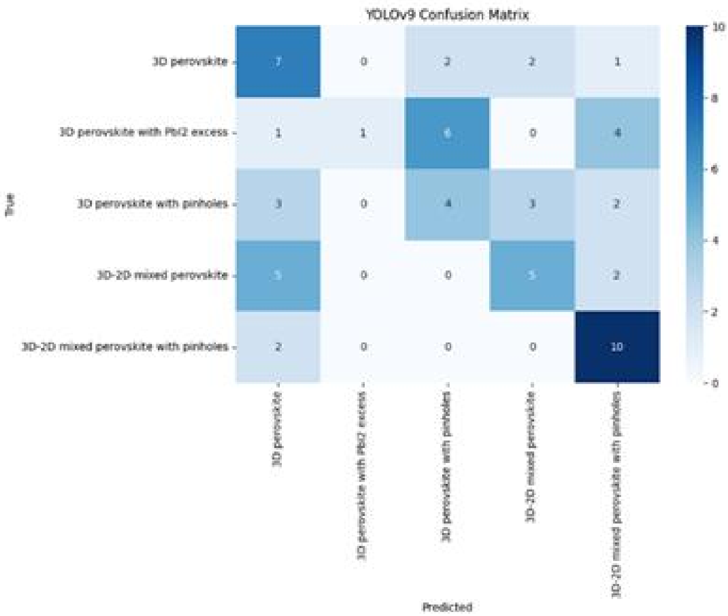

Figure 6. Confusion matrix detailed for different perovskite categories for YOLOv9

Additionally, in the final phase of our study, we deployed the defect classifier as a Streamlit-based web application, showcasing its practical utility and flexibility for real-time analysis of perovskite solar cell SEM images. This tool allows researchers to upload SEM images and receive immediate defect predictionssuch as 3D perovskite with pinholes or 3D-2D mixed perovskitealongside confidence scores and descriptive tooltips, enhancing transparency and encouraging critical evaluation of results. The interface, designed with usability in mind, includes visualization panels and a reference image gallery, making it accessible to laboratory technicians and researchers without deep learning expertise. Tested with our 1,250-image test set, the application consistently delivered accurate classifications (e.g., YOLOv8's 100% test accuracy) despite dataset limitations, demonstrating its potential as a valuable tool for the research community. By providing an interactive platform to analyze defect types, this web application not only bridges the gap between academic research and practical application but also offers a flexible, user-friendly solution that can be further refined and expanded, empowering researchers to explore and address material defects in perovskite solar cells effectively. This deployment underscores the adaptability of our approach and its readiness for broader adoption in both research and industrial settings. (Github Link: https://github.com/Sahilsonii/Multi-Model-Deep-Learning-Framework-for-Defect-Detection-in-Perovskite-Solar-Cell-SEM-Images)

V. CONCLUSION

This study successfully developed a multi-model deep learning framework for defect detection in perovskite solar cell SEM images, achieving notable performance despite significant dataset constraints. YOLOv8 emerged as the top performer with perfect classification on the 1,250-image test set at 75 FPS, while DenseNet169 and ResNet50V2 also excelled with approximately 96.7% accuracy, highlighting the efficacy of carefully selected architectures in limited-data scenarios. The deployment of the classifier within a Streamlit web application further demonstrated its practical utility, offering researchers a user-friendly tool to analyze defects in real time with transparency through confidence scores and visualizations. However, the primary challenge remains the inherent difficulty in collecting large-scale SEM datasets, as our dataset of 2,380–4,560 images fall short of the 50,000+ typically required for robust deep learning generalization, limiting the models' adaptability to diverse laboratory conditions. Ethical considerations, including transparency, accountability, and open-source release of code and models, ensure reproducibility and foster community collaboration to address these limitations. Future work should focus on collaborative data collection, domain adaptation, and advanced learning techniques to overcome dataset constraints, building on this foundation to fully realize the potential of automated defect detection in perovskite solar cell research and quality control.

ACKNOWLEDGEMENTS

We would like to acknowledge the contributions of all authors to this study. AS and SS were responsible for data curation, analysis, and supervision of the experimental work, including model training, evaluation, and deployment of the Streamlit web application. RS contributed to the conceptualization of the study, provided the dataset, and took the lead in writing the manuscript. Their combined efforts were instrumental in overcoming the challenges posed by limited dataset size and computational constraints, ensuring the successful completion of this research. We would further like to thank Florida International University in Miami for the immense infrastructure support and central facilities like Advanced Manufacturing Research Institute at Engineering Centre fostering cutting edge research technologies.

Conflict of Interest

Authors declare no competing interests against each other.

REFERENCES

[1]. Hui, Z., Wang, M., Yin, X., Wang, Y., & Yue, Y. (2023). Machine learning for perovskite solar cell design. *Computational Materials Science*, *226*, 112215. https://doi.org/10.1016/j.commatsci.2023.112215

[2]. Li, J., Pradhan, B., Gaur, S., & Thomas, J. (2019). Predictions and strategies learned from machine learning to develop high-performing perovskite solar cells. *Advanced Energy Materials*, *9*(35), 1901891. https://doi.org/10.1002/aenm.201901891

[3]. Chen, C., Maqsood, A., & Jacobsson, T. J. (2023). The role of machine learning in perovskite solar cell research. *Journal of Alloys and Compounds*, *960*, 170824. https://doi.org/10.1016/j.jallcom.2023.170824

[4]. Bansal, N. K., Mishra, S., Dixit, H., Porwal, S., Singh, P., & Singh, T. (2023). Machine learning in perovskite solar cells: Recent developments and future perspectives. *Energy Technology*, *11*(11), 2300735. https://doi.org/10.1002/ente.202300735

[5]. Zhi, C., Wang, S., Sun, S., Li, C., Li, Z., Wan, Z., & ... (2023). Machine-learning-assisted screening of interface passivation materials for perovskite solar cells. *ACS Energy Letters*, *8*(3), 1424–1433. https://doi.org/10.1021/acsenergylett.2c02818

[6]. Mammeri, M., Bencherif, H., Dehimi, L., & ... (2024). Stability forecasting of perovskite solar cells utilizing various machine learning and deep learning techniques. *Journal of Optics*. Advance online publication. https://doi.org/10.1007/s12596-024-01819-9

[7]. Zhang, J., Liu, B., Liu, Z., Wu, J., Arnold, S., Shi, H., Osterrieder, T., Hauch, J. A., Wu, Z., Luo, J., Wagner, J., Berger, C. G., Stubhan, T., Schmitt, F., Zhang, K., Sytnyk, M., Heumueller, T., Sutter-Fella, C. M., Peters, I. M., Zhao, Y., & Brabec, C. J. (2023). Optimizing perovskite thin-film parameter spaces with machine learning-guided robotic platform for high-performance perovskite solar cells. *Advanced Energy Materials*, *13*(45), 2302594. https://doi.org/10.1002/aenm.202302594

[8]. Liu, Z., & ... (2022). Machine learning with knowledge constraints for process optimization of open-air perovskite solar cell manufacturing. *Joule*, *6*(4), 834–849. https://doi.org/10.1016/j.joule.2022.03.003

[9]. Liu, Y., Tan, X., Liang, J., Han, H., Xiang, P., & Yan, W. (2023). Machine learning for perovskite solar cells and component materials: Key technologies and prospects. *Advanced Functional Materials*, *33*(27), 2214271. https://doi.org/10.1002/adfm.202214271

[10]. Liu, Y., Tan, X., Xiang, P., Tu, Y., Shao, T., Zang, Y., Li, X., & Yan, W. (2024). Machine learning as a characterization method for analysis and design of perovskite solar cells. *Materials Today Physics*, *42*, 101359. https://doi.org/10.1016/j.mtphys.2024.101359

[11]. Subba, S., Rai, P., & Chatterjee, S. (2025). Machine learning approaches in advancing perovskite solar cells research. *Advanced Theory and Simulations*, *8*(1), 2400652. https://doi.org/10.1002/adts.202400652

IJARSCT
International Journal of Advanced Research in Science, Communication and Technology
International Open-Access, Double-Blind, Peer-Reviewed, Refereed, Multidisciplinary Online Journal
ISSN: 2581-9429
Volume 5, Issue 7, June 2025
Impact Factor: 7.67
[12]. Malek, I. I., Imtiaz, H., & Subrina, S. (2024). Machine learning driven performance enhancement of perovskite solar cells with CNT as both hole transport layer and back contact. *Solar Energy*, *278*, 112737. https://doi.org/10.1016/j.solener.2024.112737

[13]. Hu, Y., Hu, X., Zhang, L., Zheng, T., You, J., Jia, B., Ma, Y., Du, X., Zhang, L., Wang, J., Che, B., Chen, T., & Liu, S. (2022). Machine-learning modeling for ultra-stable high-efficiency perovskite solar cells. *Advanced Energy Materials*, *12*(36), 2201463. https://doi.org/10.1002/aenm.202201463

[14]. Salah, M. M., Ismail, Z., & Abdellatif, S. (2023). Selecting an appropriate machine-learning model for perovskite solar cell datasets. *Materials for Renewable and Sustainable Energy*, *12*, 187–198. https://doi.org/10.1007/s40243-023-00239-2

[15]. Kusuma, F. J., Widianto, E., Wahyono, Santoso, I., Sholihun, Absor, M. A. U., Sakti, S. P., &Triyana, K. (2025). Optimizing novel device configurations for perovskite solar cells: Enhancing stability and efficiency through machine learning on a large dataset. *Renewable Energy*, *247*, 122947. https://doi.org/10.1016/j.renene.2025.122947

[16]. Zhou, H., Wang, K., Nie, C., Deng, J., Chen, Z., Zhang, K., Zhao, X., Liang, J., Huang, D., Zhao, L., Jang, H. S., & Kong, J. (2025). Quantitative analysis of perovskite morphologies employing deep learning framework enables accurate solar cell performance prediction. *Small*, *21*(4), 2408528. https://doi.org/10.1002/smll.202408528

[17]. Vakharia, V., Shah, M., Suthar, V., Patel, V. K., & Solanki, A. (2023). Hybrid perovskites thin films morphology identification by adapting multiscale-SinGAN architecture, heat transfer search optimized feature selection and machine learning algorithms. *Physica Scripta*, *98*(2), 025203. https://doi.org/10.1088/1402-4896/acae49

[18]. Massuyeau, F., Broux, T., Coulet, F., Demessence, A., Mesbah, A., & Gautier, R. (2022). Perovskite or not perovskite? A deep-learning approach to automatically identify new hybrid perovskites from X-ray diffraction patterns. *Advanced Materials*, *34*(39), 2203879. https://doi.org/10.1002/adma.202203879

[19]. Zhang, Y., & ... (2024). Machine learning quantification of grain characteristics for perovskite solar cells. *Matter*, *7*(1), 255–265. https://doi.org/10.1016/j.matt.2023.10.032

[20]. Marchenko, E. I., Korolev, V. V., Kobeleva, E. A., Belich, N. A., Udalova, N. N., Eremin, N. N., & ... (2025). Machine learning recognition of hybrid lead halide perovskites and perovskite-related structures from X-ray diffraction patterns. *Nanoscale*, *17*(5), 2742–2752. https://doi.org/10.1039/D4NR04531A

[21]. Li, Z., Nega, P. W., Nellikkal, M. A. N., Dun, C., Zeller, M., Urban, J. J., & ... (2022). Dimensional control over metal halide perovskite crystallization guided by active learning. *Chemistry of Materials*, *34*(2), 756–767. https://doi.org/10.1021/acs.chemmater.1c03564

[22]. Lee, H. B., Kumar, N., Devaraj, V., Tyagi, B., He, S., Sahani, R., Ko, K., Oh, J., & Kang, J. (2021). Trifluoromethyl-group bearing, hydrophobic bulky cations as defect passivators for highly efficient, stable perovskite solar cells. *Solar RRL*, *5*(10), 2100712. https://doi.org/10.1002/solr.202100712

[23]. Sahani, R., Kumar, N., Perini, C. A. R., Rahmani, A., Muñoz, D., LaFollette, D., Lawton, J., Datta, K., Li, R., Correa-Baena, J.-P., Jurca, T., Lai, C.-Y., & Radu, D. R. (2025). 2D/3D heterostructure halide perovskite thin films through an innovative spray-deposition of bulky organic cation-containing ammonium salts. *Advanced Materials Interfaces*, *12*(5), 2400823. https://doi.org/10.1002/admi.202400823

[24]. Gu, G. H., Jang, J., & Noh, J. (2022). Perovskite synthesizability using graph neural networks. *npj Computational Materials*, *8*, 71. https://doi.org/10.1038/s41524-022-00757-z

[25]. Huang, J., & Ling, C. X. (2005). Using AUC and accuracy in evaluating learning algorithms. *IEEE Transactions on Knowledge and Data Engineering*, *17*(3), 299–310. https://doi.org/10.1109/TKDE.2005.50

[26]. Green, M., Ho-Baillie, A., & Snaith, H. (2014). The emergence of perovskite solar cells. *Nature Photonics*, *8*, 506–514. https://doi.org/10.1038/nphoton.2014.134

[27]. Lee, M. M., Teuscher, J., Miyasaka, T., Murakami, T. N., & Snaith, H. J. (2012). Efficient hybrid solar cells based on meso-superstructured organometal halide perovskites. *Science*, *338*(6107), 643–647. https://doi.org/10.1126/science.1228604

IJARSCT
International Journal of Advanced Research in Science, Communication and Technology
International Open-Access, Double-Blind, Peer-Reviewed, Refereed, Multidisciplinary Online Journal
ISSN: 2581-9429
Volume 5, Issue 7, June 2025
Impact Factor: 7.67

Supporting Information

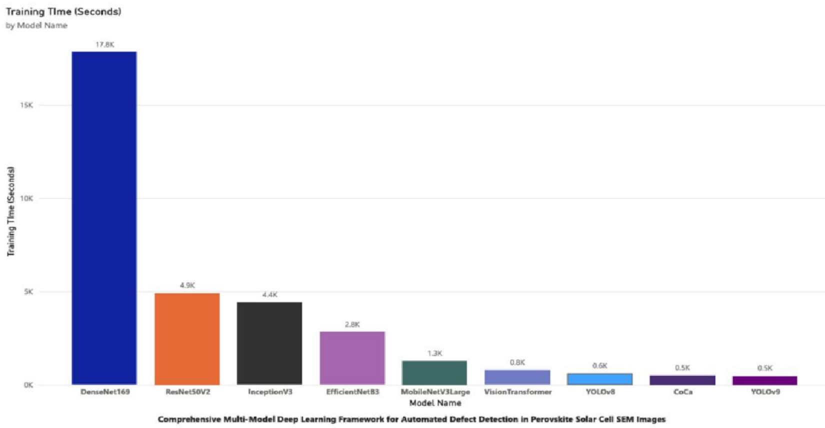

Figure S1. Training time comparison based on different models applied

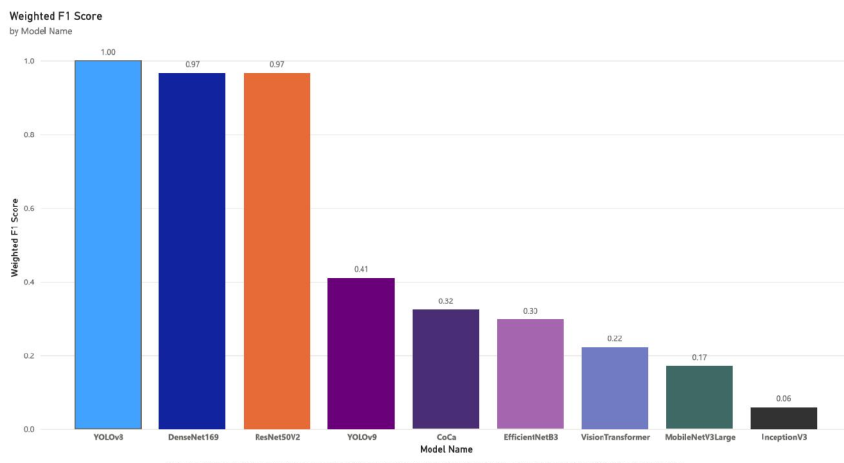

Figure S2. Weighted F1-score comparison based on different models applied

DOI: 10.48175/IJARSCT-28026

IJARSCT
International Journal of Advanced Research in Science, Communication and Technology
International Open-Access, Double-Blind, Peer-Reviewed, Refereed, Multidisciplinary Online Journal
Volume 5, Issue 7, June 2025
ISSN: 2581-9429
Impact Factor: 7.67

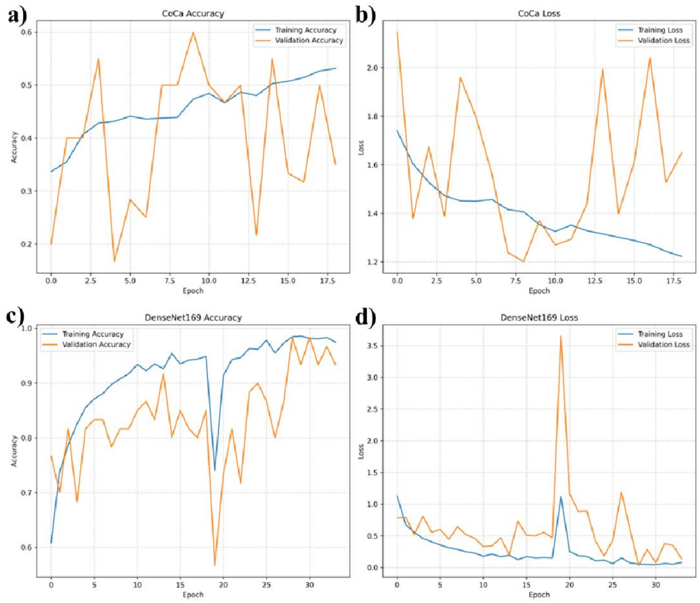

Figure S3. Accuracy and loss parameters for a) CoCa and b) DenseNet169 models

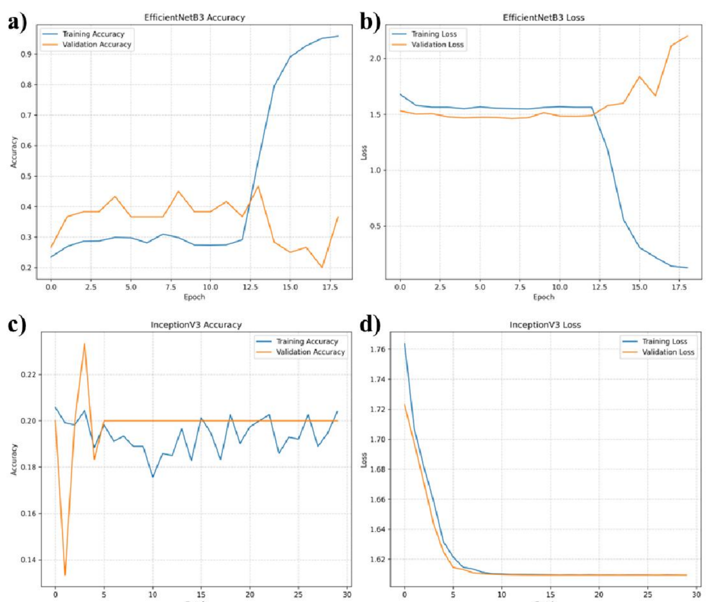

Figure S4. Accuracy and loss parameters for a) EfficientNetB3 and b) InceptionV3 models

DOI: 10.48175/IJARSCT-28026

IJARSCT
International Journal of Advanced Research in Science, Communication and Technology
International Open-Access, Double-Blind, Peer-Reviewed, Refereed, Multidisciplinary Online Journal
ISSN: 2581-9429
Volume 5, Issue 7, June 2025
Impact Factor: 7.67

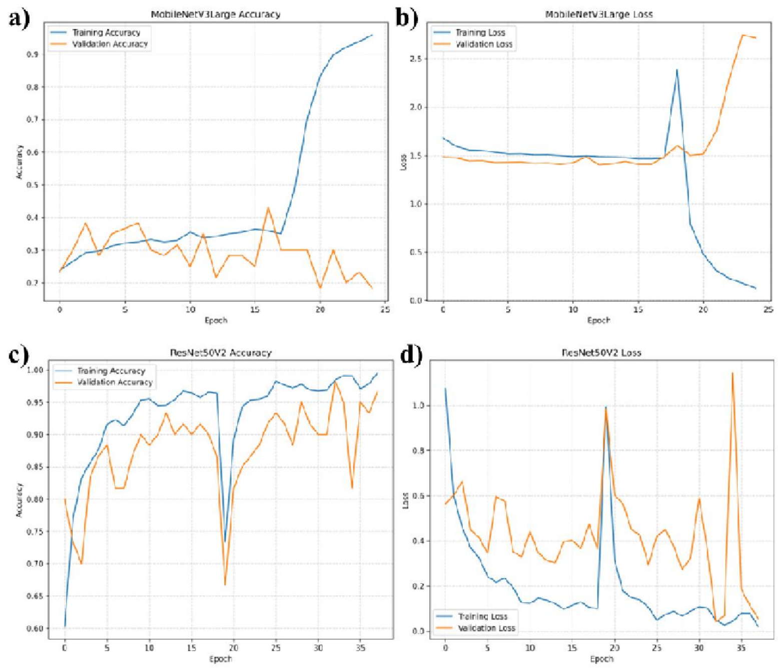

Figure S5. Accuracy and loss parameters for a) MobileNetV3Large and b) ResNet50V2 models

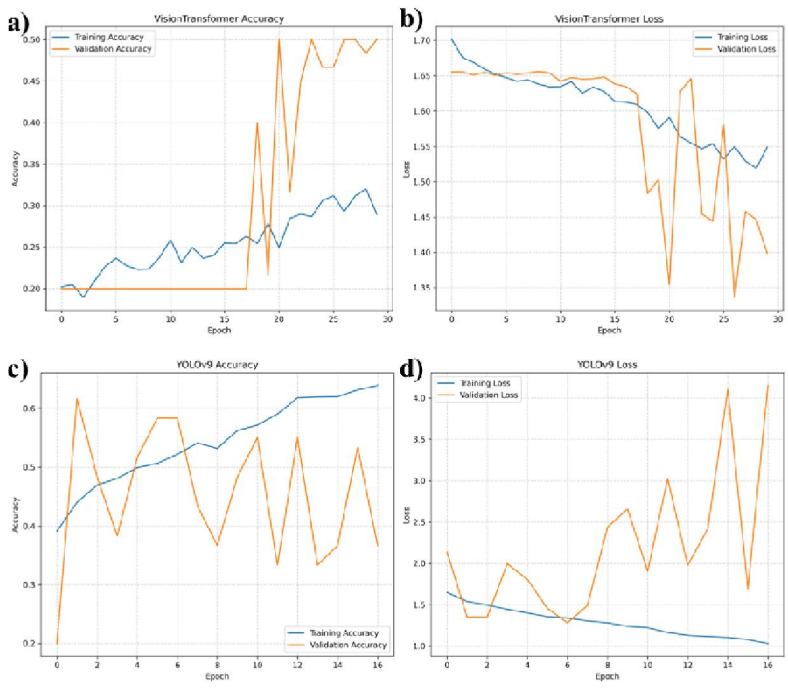

Figure S6. Accuracy and loss parameters for a) VisionTransformer and b) YOLOv9 models

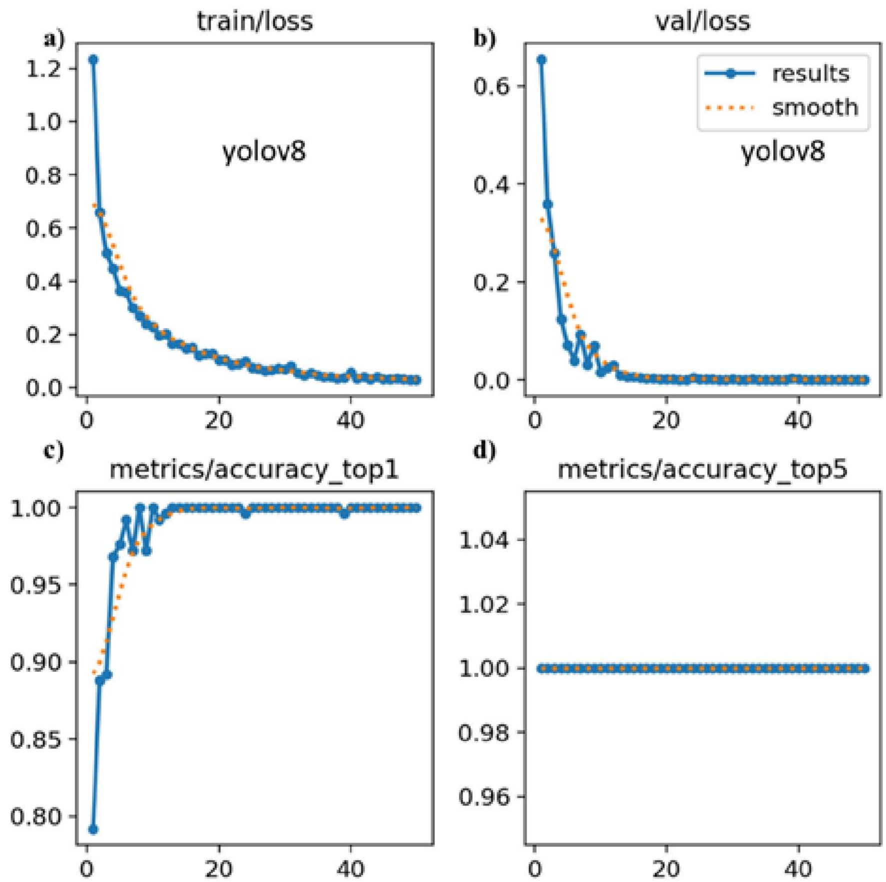

Figure S7. Accuracy and loss parameters for YOLOv8

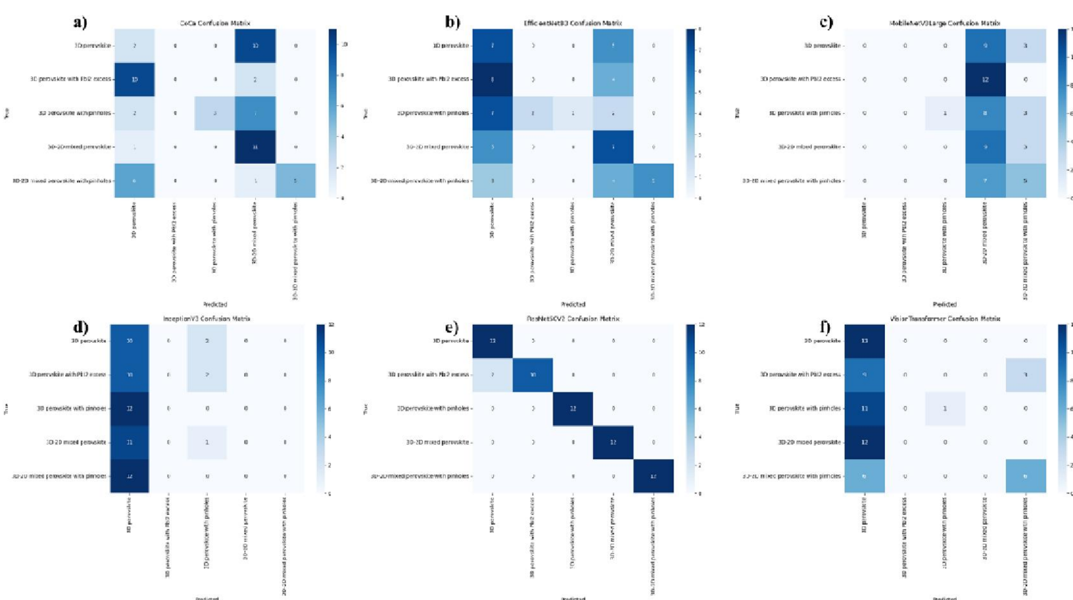

Figure S8. Confusion matrix results for different models